Science Advances
AAAS

Supplementary Materials for

Lipid droplet turnover at the lysosome inhibits growth of hepatocellular carcinoma in a BNIP3-dependent manner

Damian E. Berardi *et al.*

Corresponding author: Kay F. Macleod, kmacleod@uchicago.edu

Sci. Adv. **8**, eabo2510 (2022)
DOI: 10.1126/sciadv.abo2510

This PDF file includes:

Figs. S1 to S10

Supplemental figure 1

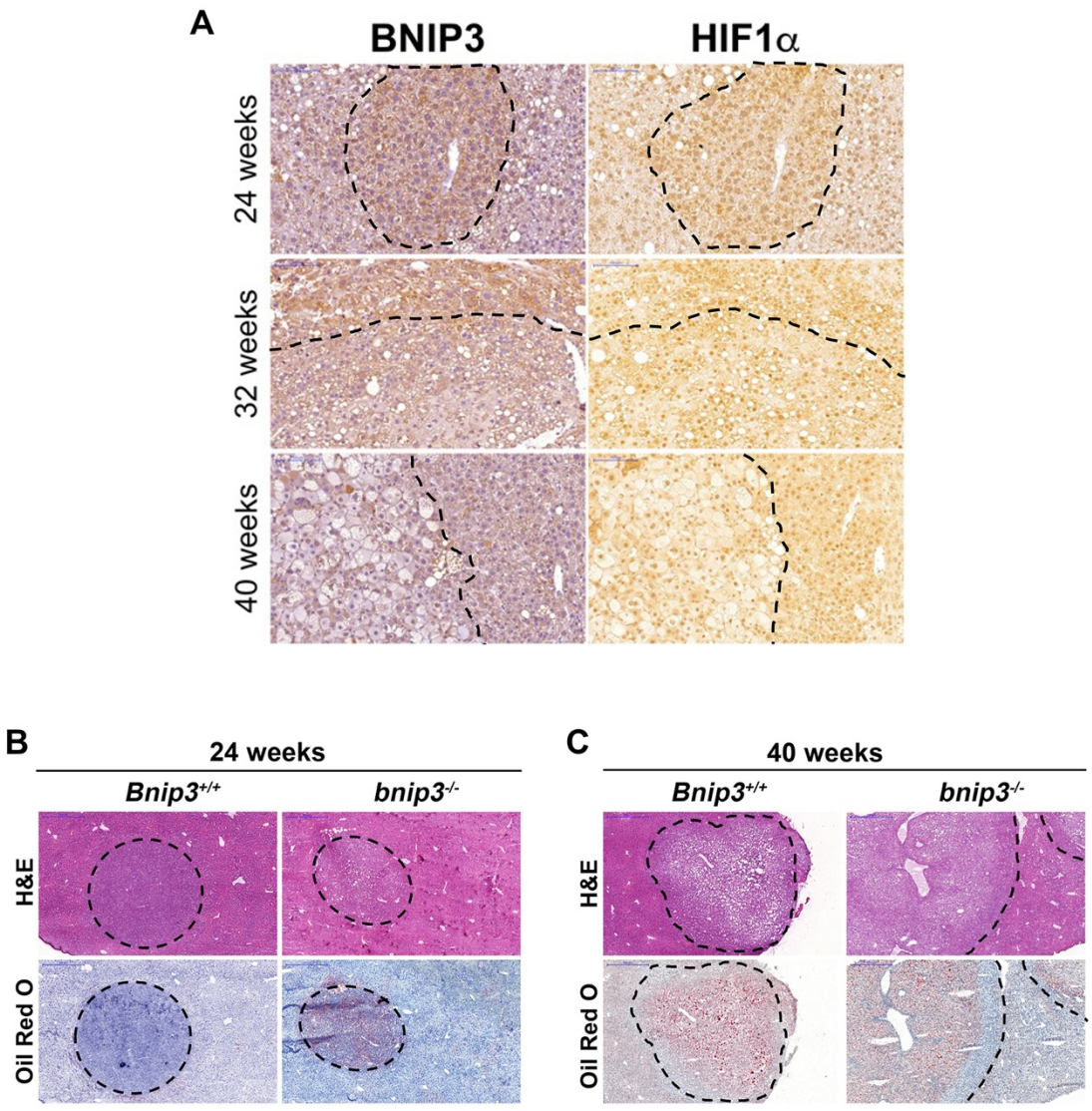

Suppl. Fig. 1. Hif-1α is upregulated in HCC tumors at early stages. (**A**) Immunohistochemical staining for BNIP3 and HIF1α in liver sections from *Bnip3*$^{+/+}$ (red) and *bnip3*$^{-/-}$ (blue) mice at 24, 32 and 40 weeks following DEN injection. Scale bars (top left) = 100 μm. (**B, C**) Liver tumor sections from *Bnip3*$^{+/+}$ and *bnip3*$^{-/-}$ mice at 24 weeks (**B**) and 40 weeks (**C**) of age following DEN injection, stained with hematoxylin & eosin (top) or Oil Red O (bottom) at 50x magnification. Scale bars (top left) = 500 μm.

Supplemental Figure 2

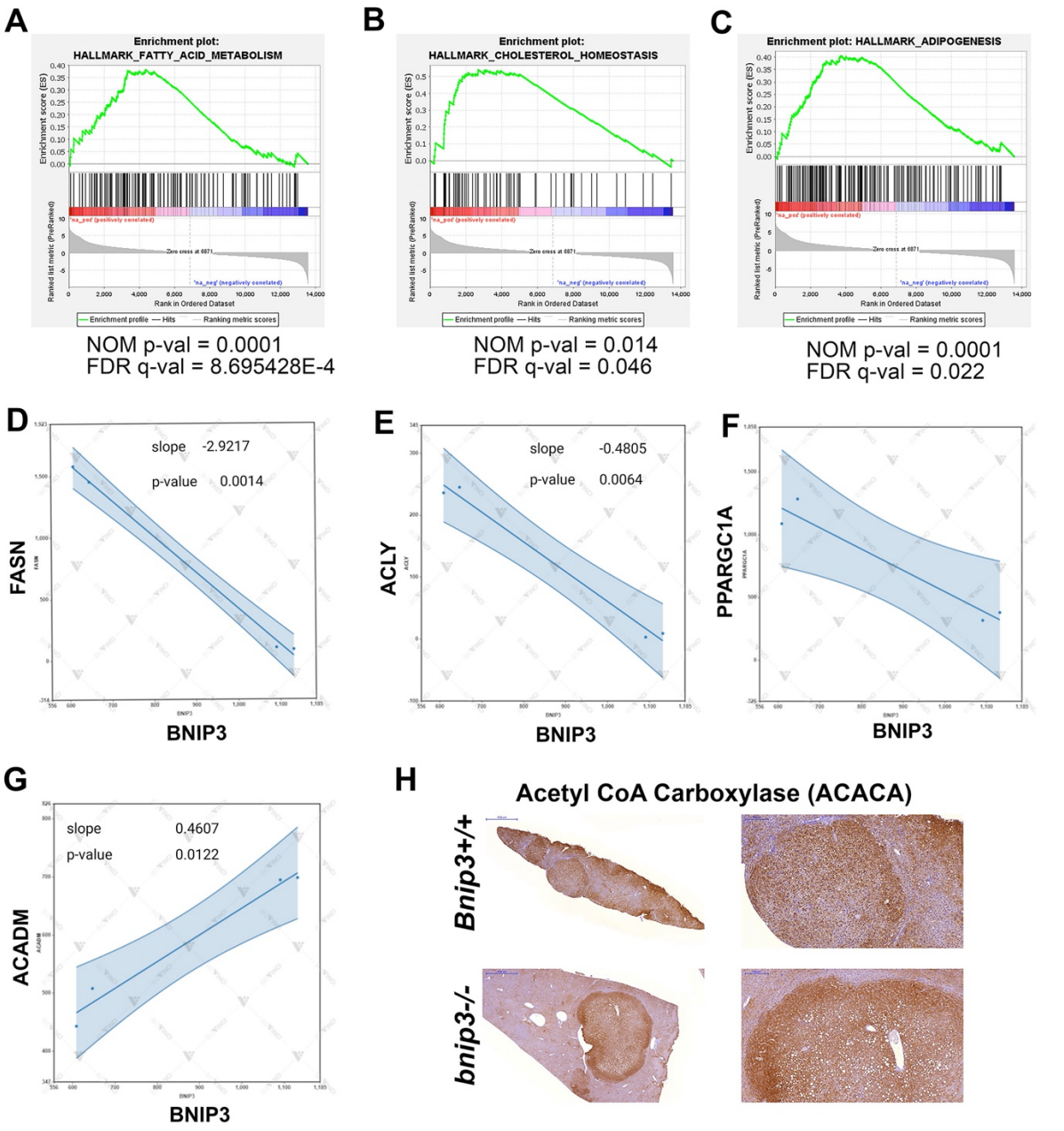

Suppl. Fig. 2. BNIP3 levels in human HCC are inversely related to expression of lipogenic genes. (**A** - **C**) Gene Set Enrichment Analysis for Healthy Tissue Human Liver Biopsy (GSM2653819 and GSM2653820) Vs HCC Tissue Human Liver Biopsy (GSM2653823 and GSM2653824) from the GSE84073 RNA-Seq dataset. (**D**) Linear regression correlation analysis between BNIP3 and FASN. (**E**) Linear regression correlation analysis between BNIP3 and ACLY**.** (**F**) Linear regression correlation analysis between BNIP3 and PPARGC1A**.** (**G**) Linear regression correlation analysis between BNIP3 and ACADM. (**H**) Immunohistochemical staining for ACACA in liver sections from *Bnip3*$^{+/+}$ (red) and *bnip3*$^{-/-}$ (blue) mice at 24 weeks following DEN injection. Scale bars (top left) = 1,000 μm (left panels) and 200 μm (right panels).

Supplemental figure 3

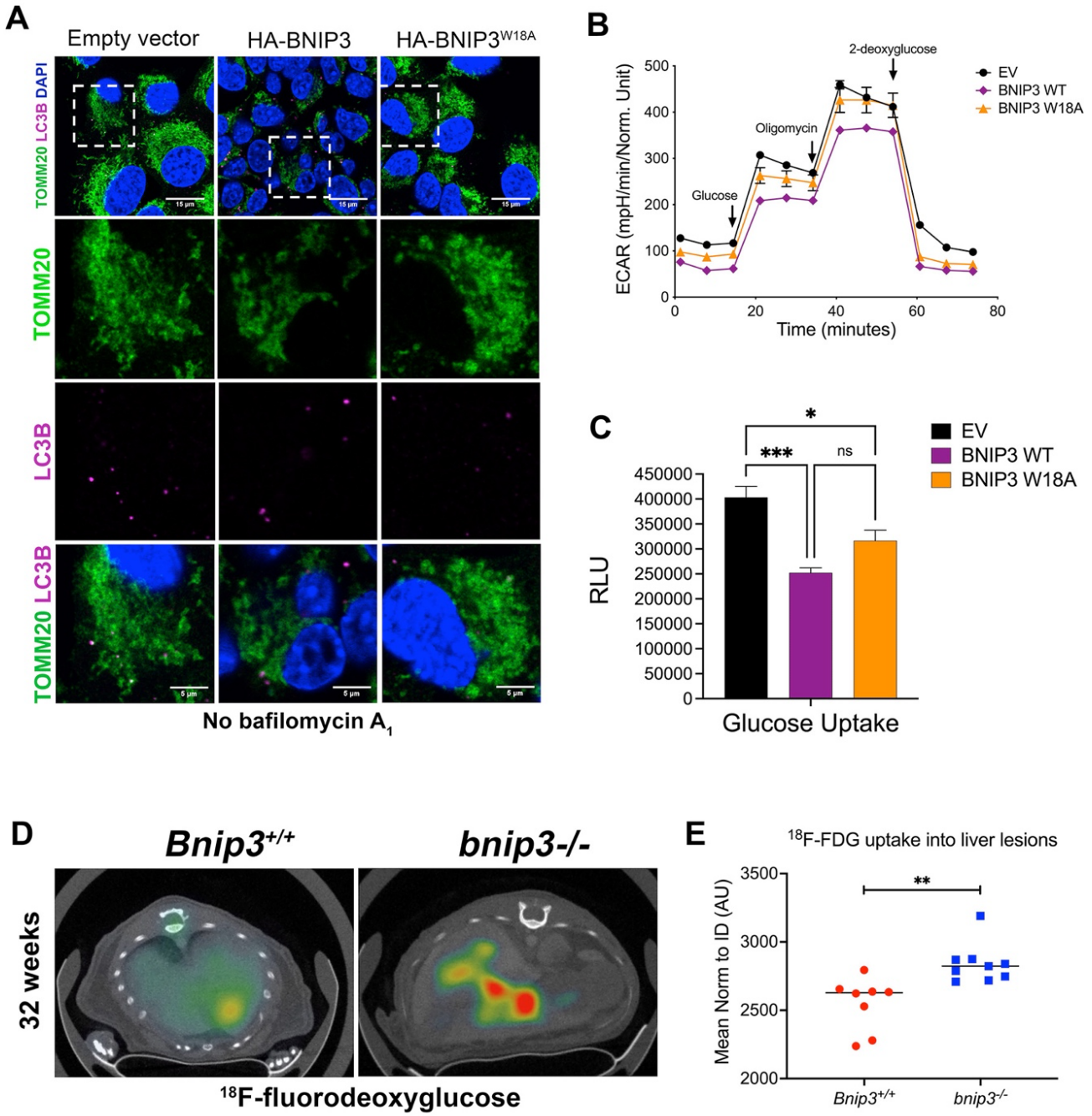

Suppl. Fig. 3. (**A**) Immunofluorescent staining for TOMM20 and LC3 in *bnip3*$^{-/-}$ HCC cells reconstituted with EV, HA-BNIP3^{WT} or HA-BNIP3^{W18A} grown in the absence of bafilomycin A_1. Scale bars shown (top) = 15 μm. Higher magnification images below, scale bars (bottom) = 5 μm. (**B**) ECAR by *bnip3*$^{-/-}$ HCC cells reconstituted with EV, HA-BNIP3^{WT} or HA-BNIP3^{W18A} in a glycolysis stress test performed on the Seahorse XF96 extracellular flux analyzer. (**C**) Glucose uptake by *bnip3*$^{-/-}$ HCC cells reconstituted with EV, HA-BNIP3^{WT} or HA-BNIP3^{W18A}. (**D**) Positron emission tomography (PET) of uptake of ^{18}F-FDG by HCC tumors in the livers of *Bnip3*$^{+/+}$ and *bnip3*$^{-/-}$ mice at 32 weeks following I.P. injection with 25 mg/kg DEN. (**E**) Quantification of ^{18}F-FDG uptake by HCC tumors in the livers of *Bnip3*$^{+/+}$ and *bnip3*$^{-/-}$ mice at 32 weeks (n = 6 per genotype; ** = $p < 0.01$).

Supplemental figure 4

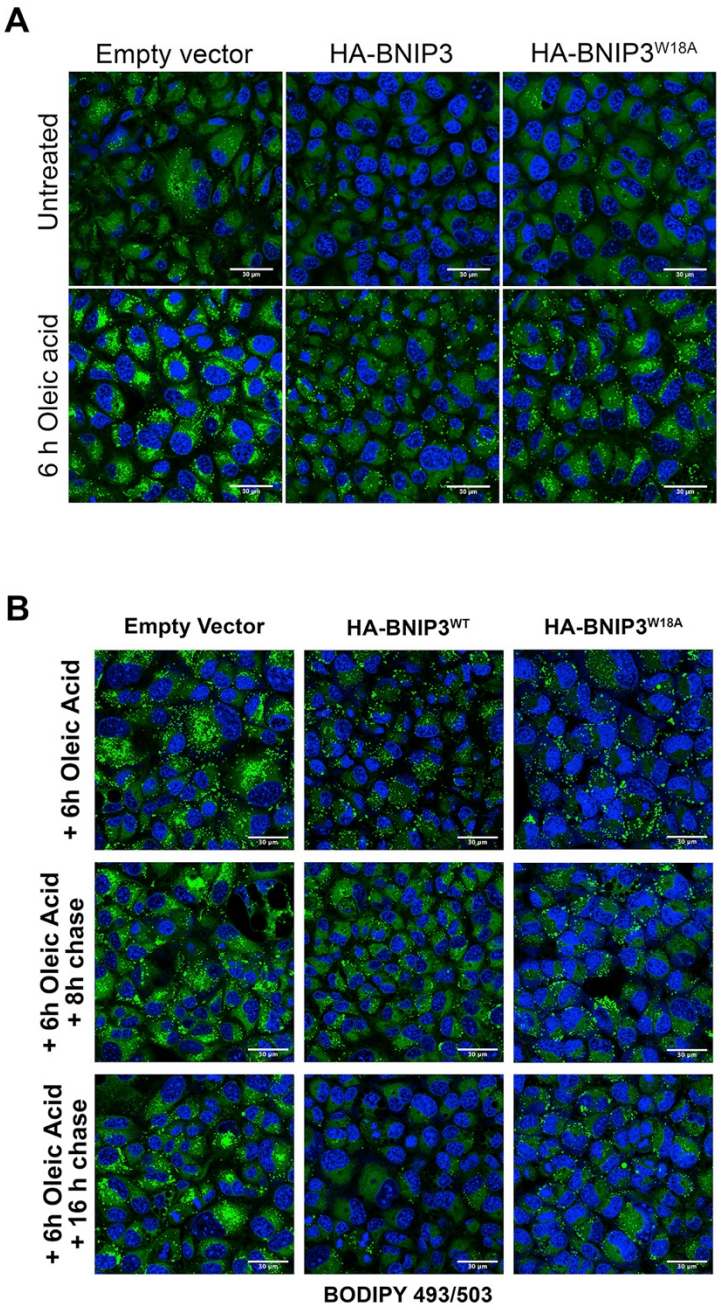

Suppl. Fig. 4. (**A**) Lipid droplet staining (BODIPY 493/503) in *bnip3*$^{-/-}$ HCC cells reconstituted with EV, HA-BNIP3^{WT} or HA-BNIP3^{W18A} +/- 100 μM oleic acid. (**B**) Lipid droplet staining (BODIPY 493/503) in *bnip3*$^{-/-}$ HCC cells reconstituted with EV, HA-BNIP3^{WT} or HA-BNIP3^{W18A} grown for 6 hrs in 100 μM oleic acid, then released into lipid free media for 0, 8 and 16 hours.

Supplemental figure 5

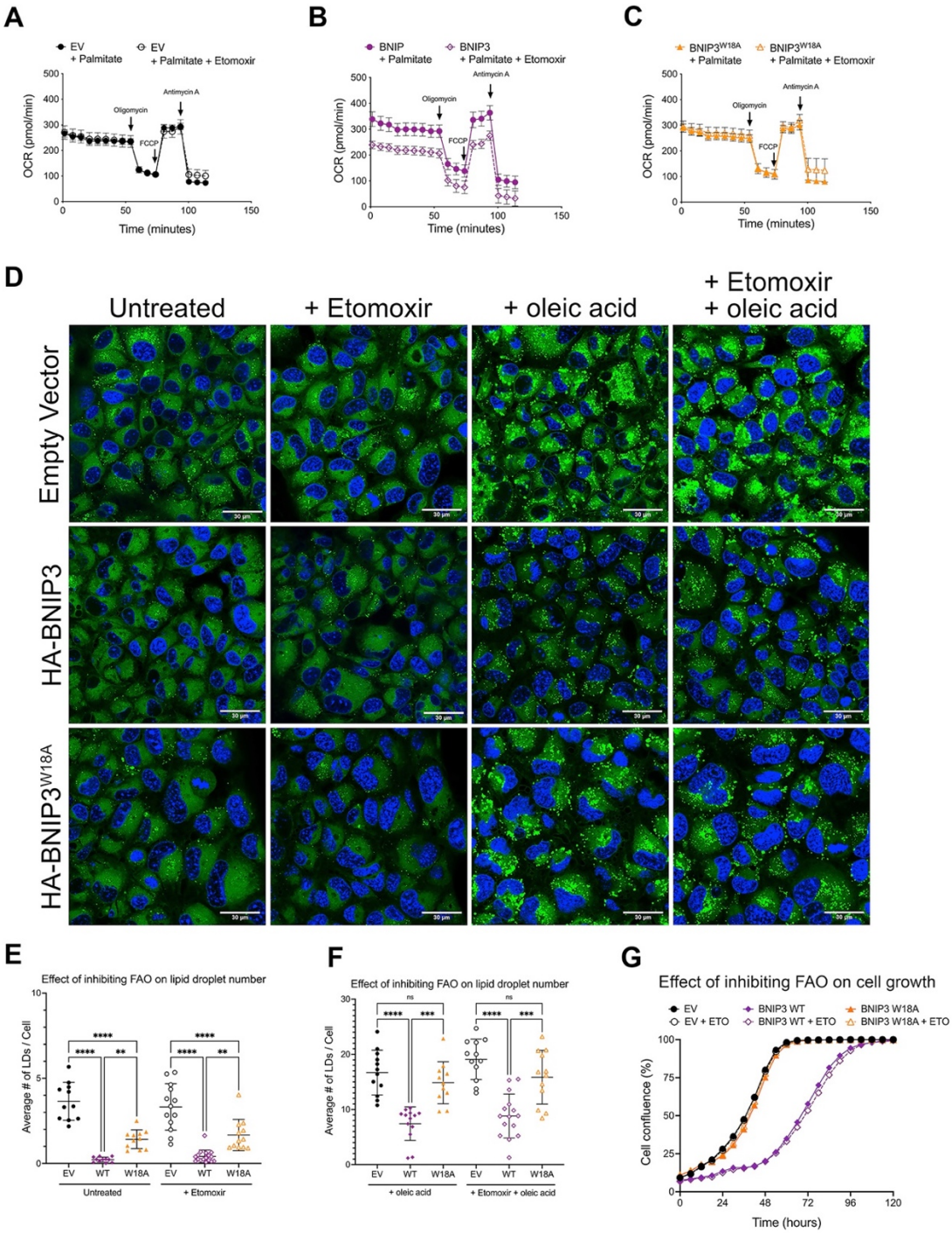

Suppl. Fig. 5. Effects of BNIP3 on fatty acid oxidation. (**A**) OCR (166 μM palmitate, 2 mM D-glucose) of *bnip3*$^{-/-}$ HCC cells reconstituted with EV +/- 10 μM Etomoxir; (**B**) OCR (166 μM palmitate, 2 mM D-glucose) in *bnip3*$^{-/-}$ HCC cells reconstituted with BNIP3^{WT} +/- 10 μM Etomoxir; (**C**) OCR (166 μM palmitate, 2 mM D-glucose) in *bnip3*$^{-/-}$ HCC cells reconstituted with BNIP3^{W18A} +/- 10 μM Etomoxir; (**D**) Fluorescent microscopy imaging of BODIPY 493/503 staining in *bnip3*$^{-/-}$ HCC cells reconstituted with EV, HA-BNIP3^{WT} or HA-BNIP3^{W18A} +/- 10 μM Etomoxir +/- 100 μM oleic acid. (**E**) Graph of BODIPY 493/503 staining in *bnip3*$^{-/-}$ HCC cells reconstituted with EV, HA-BNIP3^{WT} or HA-BNIP3^{W18A} +/- 10 μM Etomoxir (NS = not significant, *** = $p < 0.001$, **** = $p < 0.0001$;). (**F**) Graph of BODIPY 493/503 staining in *bnip3*$^{-/-}$ HCC cells reconstituted with EV, HA-BNIP3^{WT} or HA-BNIP3^{W18A} +/- 10 μM Etomoxir + 100 μM oleic acid (NS = not significant, *** = $p < 0.001$, **** = $p < 0.0001$; at least 20 cells per field, each data point is one field, n≥10 fields per condition). (**G**) Rate of cell growth determined by IncuCyte of *bnip3*$^{-/-}$ HCC cells reconstituted with EV, HA-BNIP3^{WT} or HA-BNIP3^{W18A} +/- 10 μM Etomoxir.

Supplemental figure 6

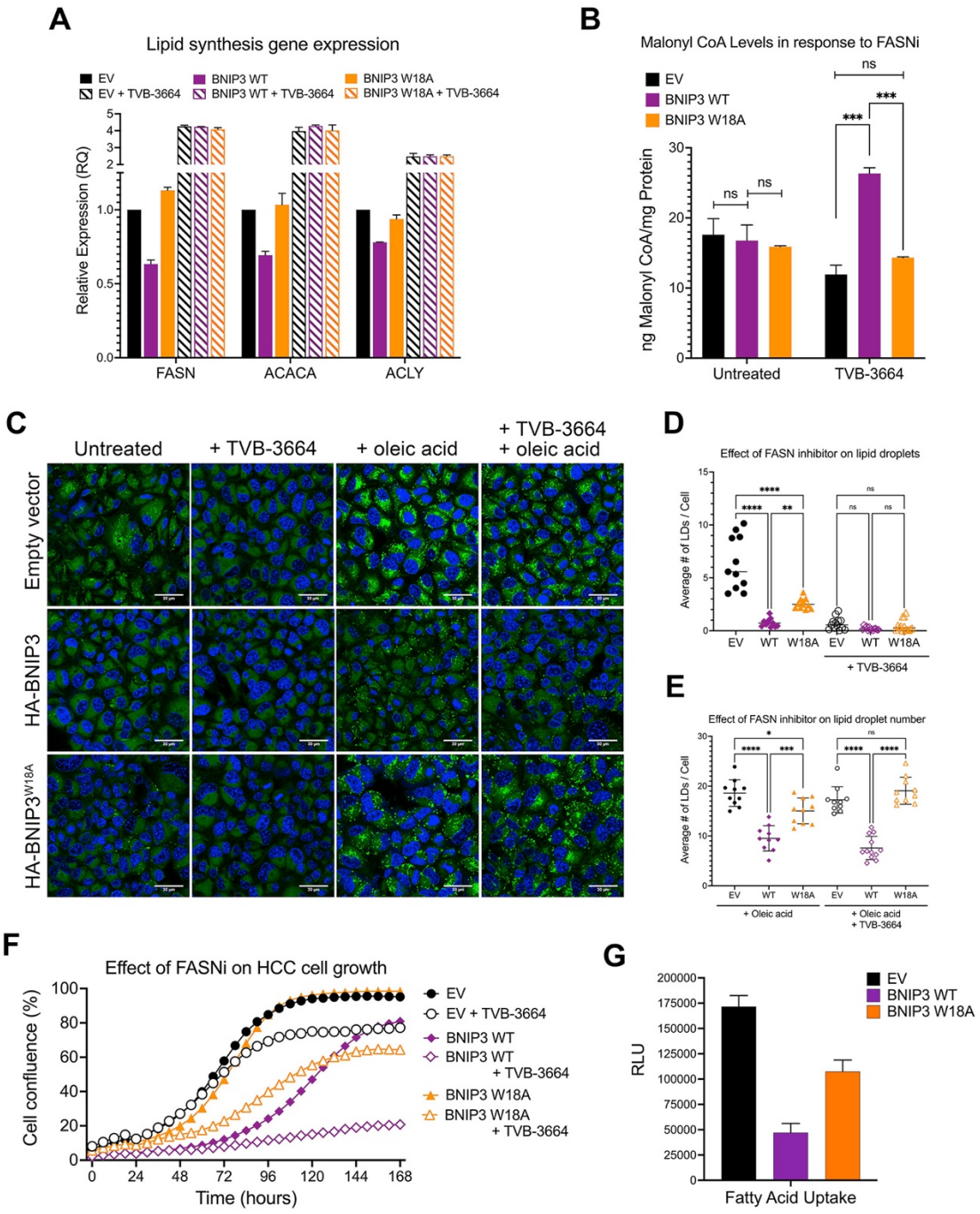

Suppl. Fig. 6. Effects of BNIP3 on lipid synthesis. (**A**) qPCR for lipogenesis genes FASN, ACLY, ACACA in *bnip3*$^{-/-}$ HCC cells reconstituted with EV, HA-BNIP3^{WT} or HA-BNIP3^{W18A} +/- TVB-3664. **B**) Graph of Malonyl CoA levels in *bnip3*$^{-/-}$ HCC cells reconstituted with EV, HA-BNIP3^{WT} or HA-BNIP3^{W18A} +/- TVB-3664 (NS = not significant, *** = $p < 0.001$). (**C**) Fluorescent microscopy imaging of BODIPY 493/503 staining in *bnip3*$^{-/-}$ HCC cells reconstituted with EV, HA-BNIP3^{WT} or HA-BNIP3^{W18A} +/- 12 nM TVB-3664 +/- 100 mM oleic acid; (**D**) Graph of BODIPY 493/503 staining in *bnip3*$^{-/-}$ HCC cells reconstituted with EV, HA-BNIP3^{WT} or HA-BNIP3^{W18A} +/- 12 nM TVB-3664 (NS = not significant, ** = $p < 0.01$, **** = $p < 0.0001$); (**E**) Graph of BODIPY 493/503 staining in *bnip3*$^{-/-}$ HCC cells reconstituted with EV, HA-BNIP3^{WT} or HA-BNIP3^{W18A} +/- 12 nM TVB-3664 + 100 mM Oleic acid (NS = not significant, * = $p < 0.05$, *** = $p < 0.001$, **** = $p < 0.0001$); At least 20 cells per field, each data point is one field, n≥10 fields per condition. (**F**) Rate of cell growth determined by IncuCyte of *bnip3*$^{-/-}$ HCC cells reconstituted with EV, HA-BNIP3^{WT} or HA-BNIP3^{W18A} +/- 12 nM TVB-3664. (**G**) Measurement of fatty acid uptake by bnip3-/- HCC cells reconstituted with EV, HA-BNIP3^{WT} or HA-BNIP3^{W18A}.

Supplemental figure 7

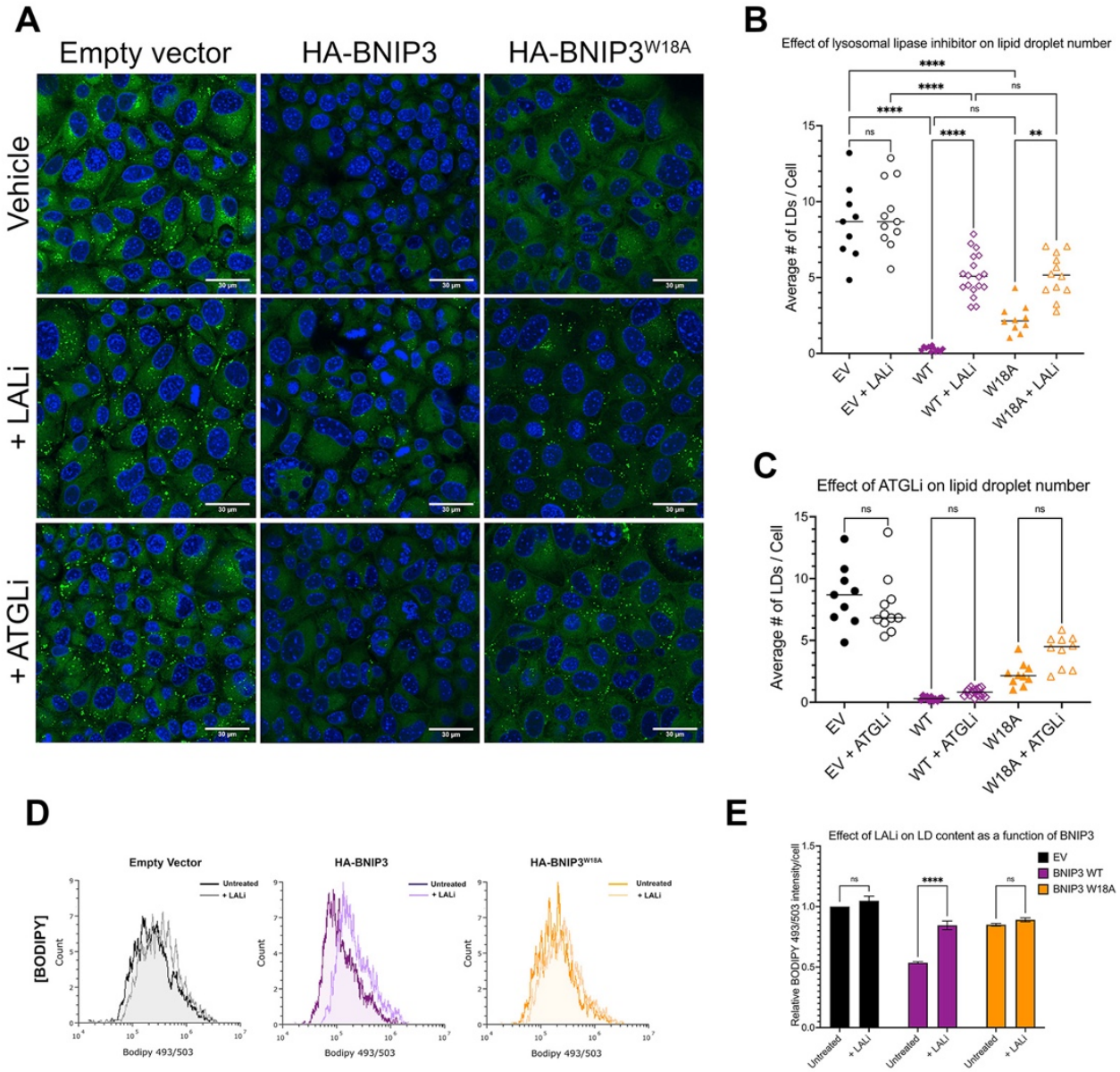

Suppl. Fig. 7. BNIP3 induced lipid decreases are inhibited by lysosomal lipase inhibition. (**A**) Fluorescent imaging of lipid droplet stained (BODIPY 493/503) *bnip3*$^{-/-}$ HCC cells reconstituted with EV, HA-BNIP3^{WT} or HA-BNIP3^{W18A} and following treatment with LALi or ATGLi. (**B**) Graph of BODIPY 493/503 staining in *bnip3*$^{-/-}$ HCC cells reconstituted with EV, HA-BNIP3^{WT} or HA-BNIP3^{W18A} following treatment with LALi (*, $p < 0.05$; ****, $p < 0.0001$). (**C**) Graph of BODIPY 493/503 staining in *bnip3*$^{-/-}$ HCC cells reconstituted with EV, HA-BNIP3^{WT} or HA-BNIP3^{W18A} following treatment with ATGLi (*, $p < 0.05$; ****, $p < 0.0001$; At least 20 cells per field, each data point is one field, n≥10 fields per condition). (**D**) Quantification of BODIPY 493/503 Imagestream analysis of *bnip3*$^{-/-}$ HCC cells reconstituted with EV, HA-BNIP3^{WT} or HA-BNIP3^{W18A} +/- 50 μM LALi. (**E**) Graph summarizing imagestream analysis of BODIPY staining of *bnip3*$^{-/-}$ HCC cells reconstituted with EV, HA-BNIP3^{WT} or HA-BNIP3^{W18A} +/- 50 μM LALi.

Supplemental figure 8

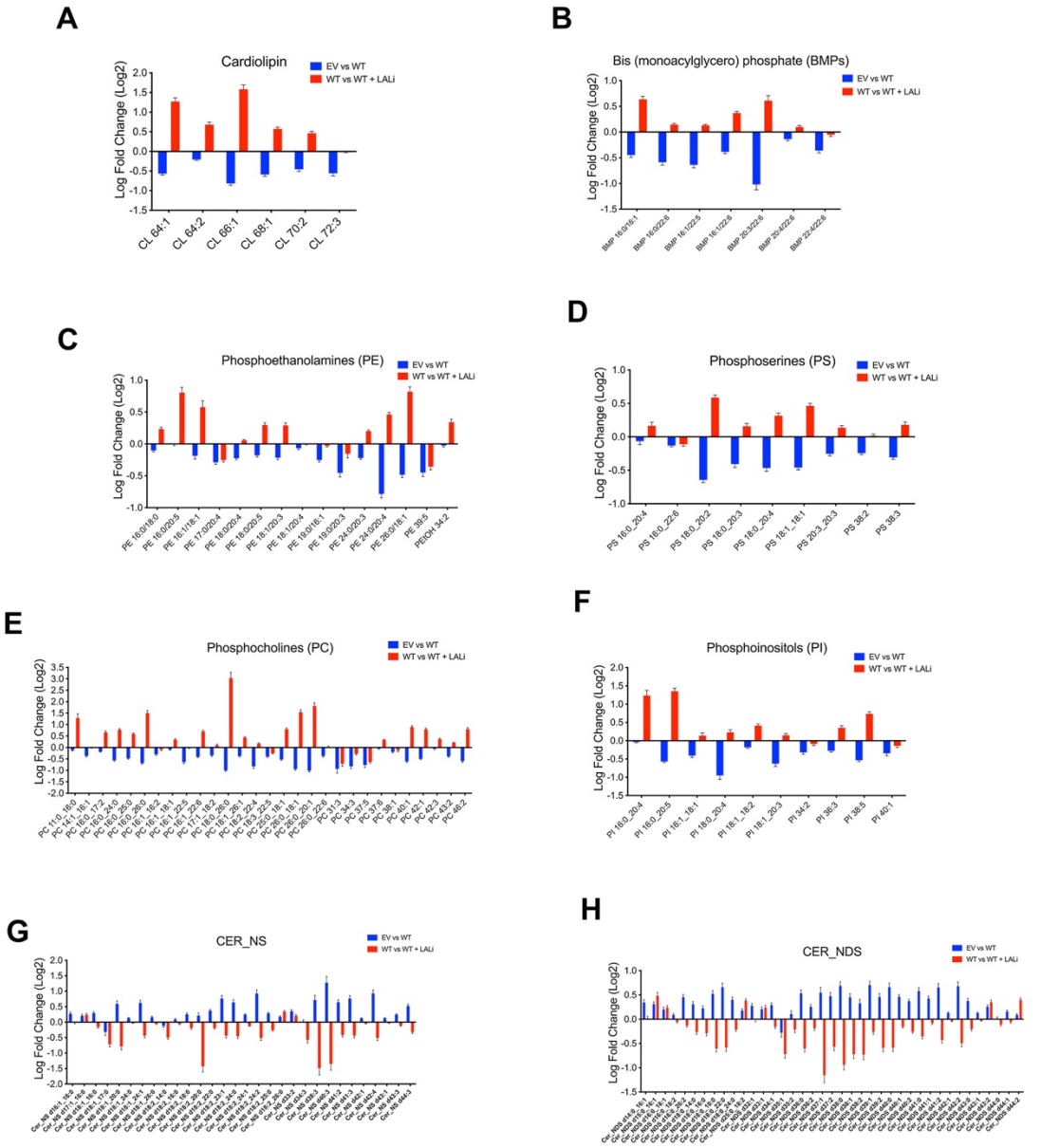

Suppl. Fig. 8. LC-MS analysis of lipid species decreased (fold change >2.0 and p> 0.05) in *bnip3*$^{-/-}$ HCC cells expressing BNIP3 WT compared to EV (blue bars) and increased by 24 hours treatment with 50 μM LALi (red bars). (**A**) Cardiolipins; (**B**) Bis (monoacylglycero) phosphates (BMPs); (**C**) Phosphoethanolamines; (**D**) Phosphoserines (PS); (**E**) Phosphocholines (PC); (**F**) Phosphoinositols (PI); (**G - H**) Ceramides.

Supplemental figure 9

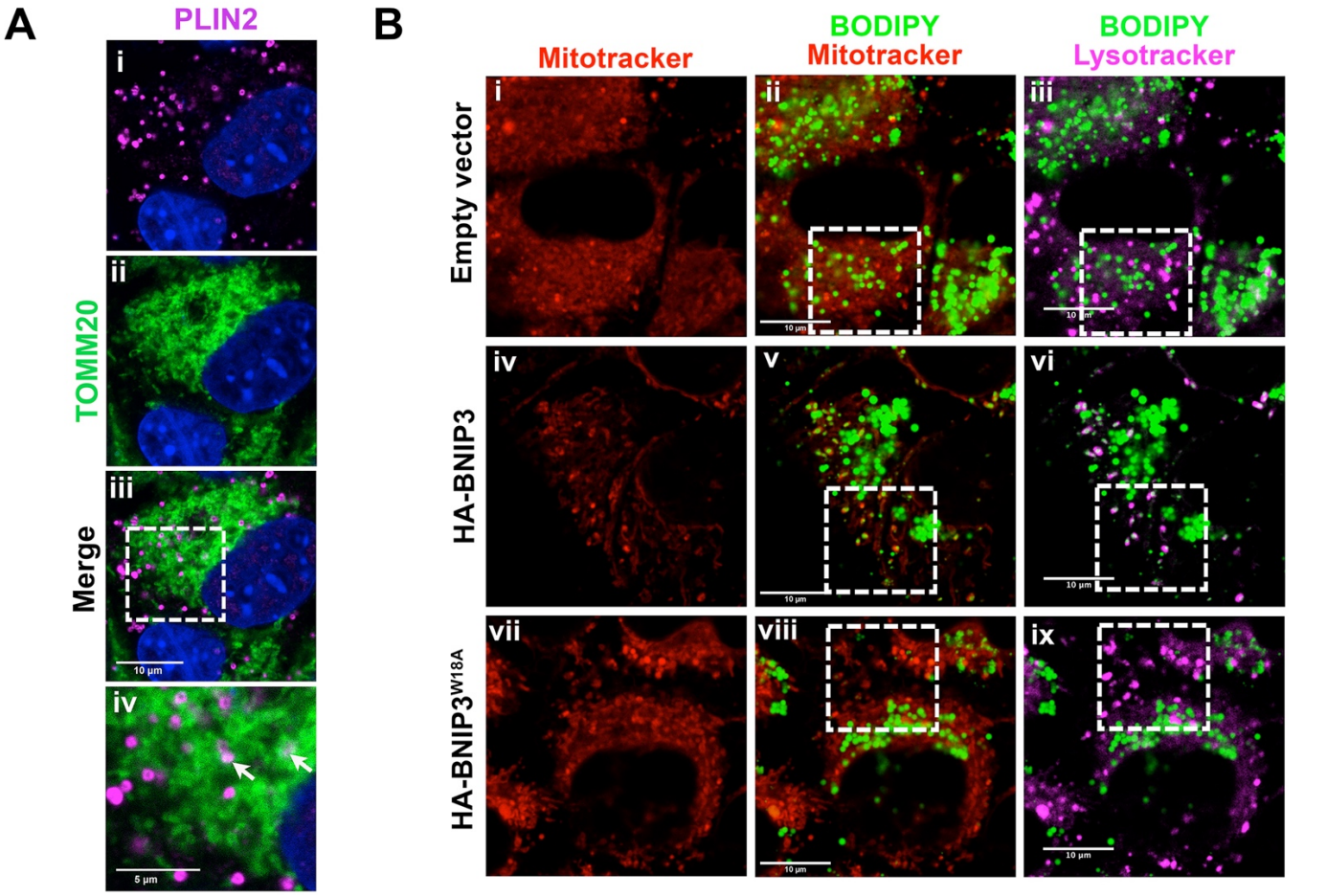

Suppl. Fig. 9. (**A**) Fluorescent microscopy of *bnip3*$^{-/-}$ HCC cells reconstituted with HA-BNIP3^{WT} and stained with antibodies to TOMM20 (green) and PLIN2 (magenta) to assess staining overlap (white, arrows in iv). White dashed square in iii indicates the area magnified in the panel iv below. (**B**) *Fluorescent* microscopy of *bnip3*$^{-/-}$ HCC cells reconstituted with EV, HA-BNIP3^{WT} or HA-BNIP3^{W18A} grown for 24 hours in 50 μM LALi + 6 hrs in 100 μM oleic acid and then stained with BODIPY 493/503 (green) and Mitotracker (red) or Lysotracker (magenta). Areas presented in figure 6G are highlighted here by the white dashed square in ii, v and viii for EV, HA-BNIP3 and HA-BNIP3^{W18A} respectively.

Supplemental figure 10

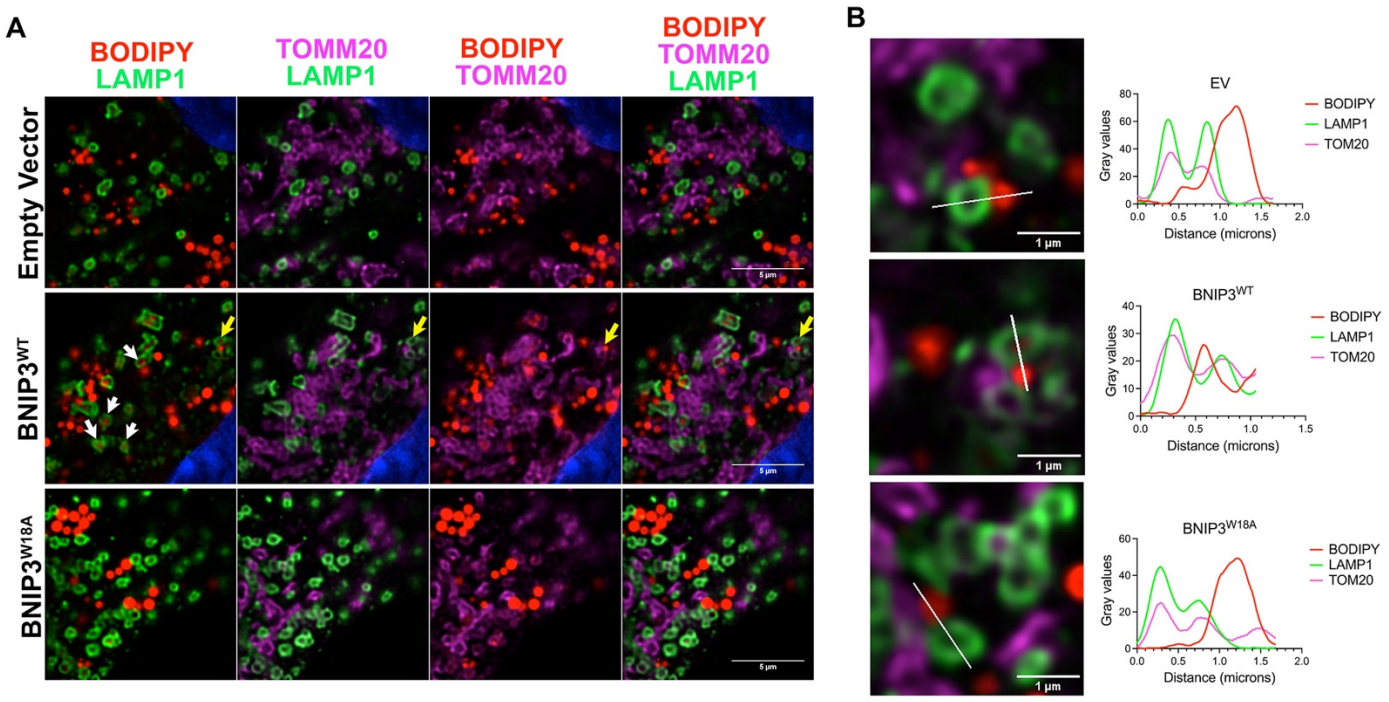

Suppl. Fig. 10. (**A**) Immunofluorescent staining of *bnip3*$^{-/-}$ HCC cells reconstituted with EV, HA-BNIP3^{WT} or HA-BNIP3^{W18A} grown for 24 hours in 50 μM LALi + 6 hrs in 100 μM oleic acid and then stained with antibodies to TOMM20 (magenta) and LAMP1 (green) and BODIPY 493/503 (red) and imaged using the laser scanning SP8 confocal microscope and lightening adaptive deconvolution programming. White arrows (middle panel) indicate representative lipid-positive lysosomes. Yellow arrow points to LD-mitochondria-lysosome interaction that is shown at high magnification in panel (**B**). (**B**) High magnification of representative images from (**A**) with associated linescan analysis of co-localization between lipid droplets (red) with mitochondria (magenta) and lysosomes (green) in *bnip3*$^{-/-}$ HCC cells reconstituted with EV, HA-BNIP3^{WT} or HA-BNIP3^{W18A}, showing that only BNIP3^{WT} (middle panel) promoted LD-mitochondria-lysosome overlap.